Electronic Supplementary Material (ESI) for Journal of Materials Chemistry C.

Construction of two-dimensional metal-organic framework with an out-of-plane magnetic anisotropy composed of single-molecule magnet

Ikumi Aratani,[a] Yoji Horii,*[a] Daisuke Takajo,[b] Yoshinori Kotani,[c] Hitoshi Osawa[c] and Takashi Kajiwara[a]

[a] *Graduate School of Humanities and Sciences, Nara Women's University, Kitauoya-Higashimachi, Nara 630-8506, Japan.*

[b] *Research Center for Thermal and Entropic Science, Graduate School of Science, Osaka University, 1-1 Machikaneyama-cho, Toyonaka, Osaka 560-0043, Japan..*

[c] *SPring-8/JASRI, Kouto, Sayo, Hyogo 679-5198, Japan.*

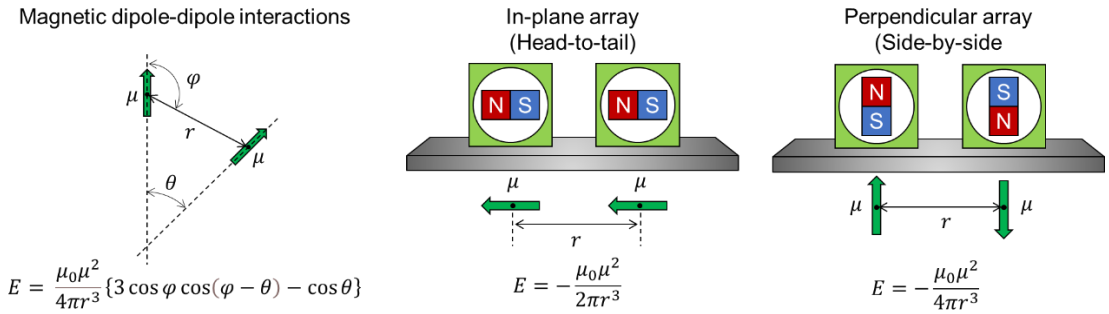

Figure S1. Magnitude of the magnetic dipole-dipole interactions in the in-plane and perpendicular array. Since the magnetism of the lanthanoid-based SMM originates from 4f orbitals that are shielded by the outer atomic orbitals (and therefore no orbital overlap between nearest SMMs), the SMM-SMM magnetic interactions are mainly driven by magnetic dipole-dipole interactions.[1] In the point-dipole approximation (this is good approximation for lanthanoid SMMs), the magnitude of magnetic dipole-dipole interaction (E) is formulated as $E = \frac{\mu_0\mu^2}{4\pi r^3}\{3\cos\varphi\cos(\varphi-\theta)-\cos\theta\}$, where μ_0 is the vacuum magnetic permeability, r is the distance between two magnetic dipoles, μ is the norm of the magnetic dipoles, θ is the angle of two magnetic dipoles, and φ is the angle between the magnetic dipole and the vector connecting two magnetic dipoles. The E value of the head-to-tail configuration seen in in-plane array is twice that of side-by-side configuration seen in the perpendicular array. Therefore, perpendicular array can supress the SMM-SMM interactions.

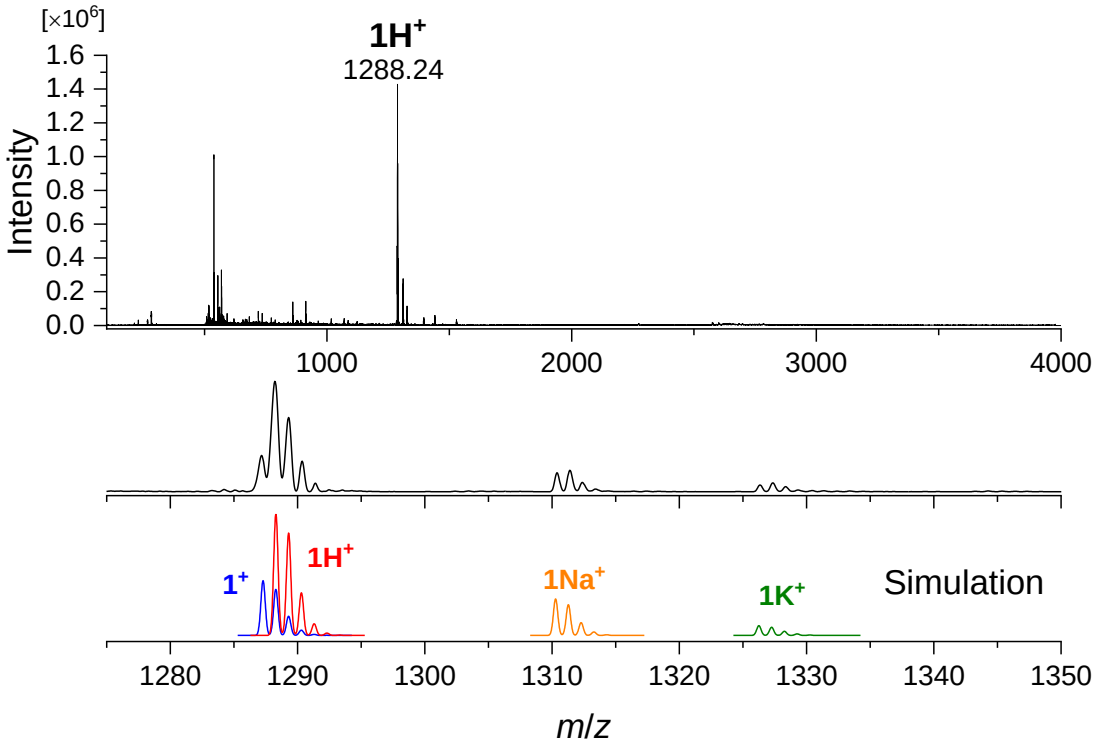

Figure S2. MALDI-TOF mass spectra for **1** using 4'-Hydroxyazobenzene-2-carboxylic Acid (HABA) as the matrix. Enlarged experimental spectra and simulated patterns for monocationic species ($\mathbf{1}^+$, $\mathbf{1}H^+$, $\mathbf{1}Na^+$ and $\mathbf{1}K^+$) were shown for comparison.

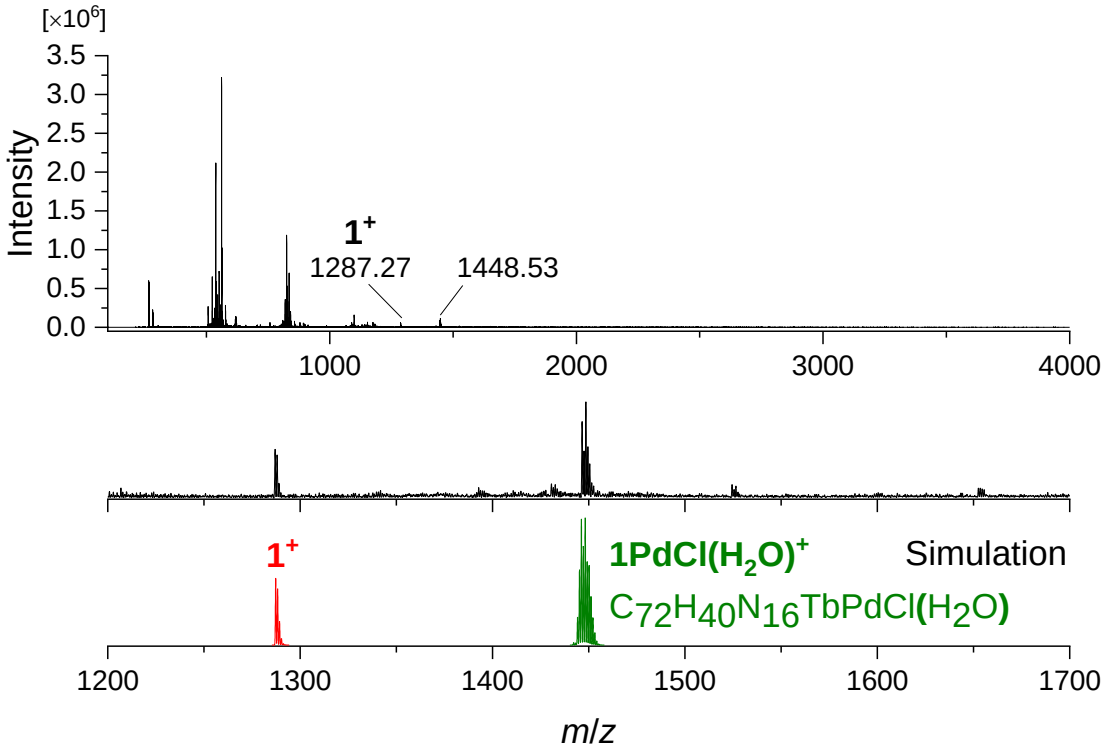

Figure S3. MALDI-TOF mass spectra for **1Pd** using 4'-Hydroxyazobenzene-2-carboxylic Acid (HABA) as the matrix. Enlarged experimental spectra and simulated patterns were shown for comparison. It is not possible to fully simulate the isotropic distribution peaks at around *m*/*z* = 1488. The similar *m*/*z* value was obtained by considering **1** with Pd, Cl and H_2O.

Table S1. **Crystalline parameters for 1.**

	1
T / K	153
Formula	$C_{74}H_{44}Cl_4N_{16}Tb$
Crystal system	Triclinic
Space group	*P*-1
Z	2
a / Å	12.7976(5)
b / Å	14.0071(6)
c / Å	18.1335(7)
α / °	93.068(3)
β / °	105.135(4)
γ / °	100.887(3)
V / Å^3	3063.1(2)
ρ / g cm^{-3}	1.581
GOF	1.035
R_1	0.0638
wR_2	0.1359
R_1 (all)	0.0995
wR_2 (all)	0.1516
CCDC number	2205797

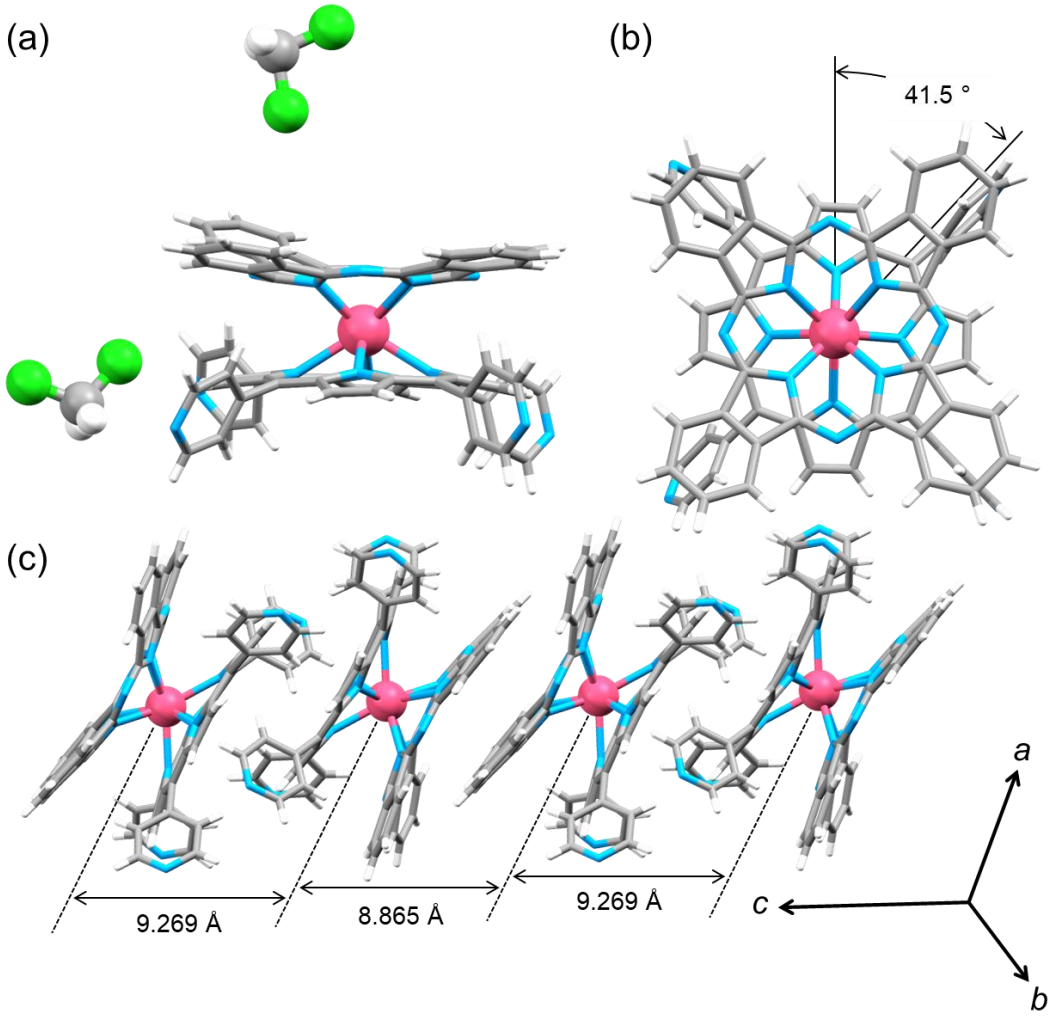

Figure S4. Crystal structure of **1** at 153 K. (a) Side view with the solvent molecules (CH_2Cl_2). (b) Top view and skew angle between Pc and TPyP. (c) Crystal packing and intermolecular Tb-Tb distances. Solvent molecules are omitted for clarity. Tb pink; Cl green; N blue; C grey, H white.

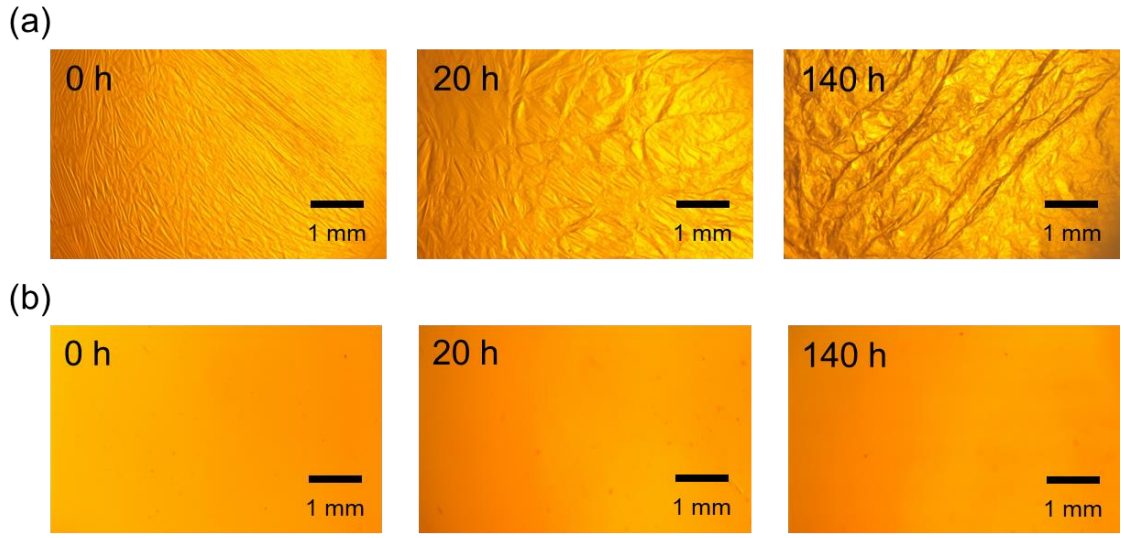

Figure S5. Optical microscope images of the liquid-liquid interface of the SMM solution and a water solution (a) with and (b) without $[PdCl_4]^-$. In the presence of $[PdCl_4]^-$, the visible thin film formed immediately at a liquid-liquid interface, indicating the formation of the MOF. The thickness of the film seemed to be increased over time. In contrast, there were no visible object without $[PdCl_4]^-$.

Table S2. Basis sets used for CASSCF calculations.

Atom	Basis set
Tb	SARC2-DKH-QZVP[2]
Coordinating N	DKH-Def2-TZVP[3]
Remaining atoms	DKH-Def2-SVP[3]

Table S3. Energy level and wavefunction composition (%) of the $^7F_6$ states of 1.

	State 1	State 2	State 3	State 4	State 5	State 6	State 7	State 8	State 9	State 10	State 11	State 12	State 13
Energy / cm^{-1}	0	0.002	245.996	246.077	344.918	355.157	358.639	361.53	365.061	381.261	395.992	401.118	403.971
M_J													
−6	50.0	50.0	0.0	0.0	0.0	0.0	0.0	0.0	0.0	0.0	0.0	0.0	0.0
−5	0.0	0.0	49.7	49.7	0.0	0.1	0.1	0.2	0.0	0.1	0.0	0.1	0.0
−4	0.0	0.0	0.1	0.1	24.8	10.5	3.2	3.1	31.6	22.6	1.1	2.1	1.0
−3	0.0	0.0	0.0	0.0	0.9	10.3	5.1	9.7	0.2	0.2	15.3	33.7	24.6
−2	0.0	0.0	0.0	0.0	0.3	2.1	14.7	21.3	10.9	0.8	23.8	5.6	20.5
−1	0.0	0.0	0.2	0.2	0.6	25.4	26.9	13.7	7.1	4.3	9.6	8.1	3.8
0	0.0	0.0	0.0	0.0	46.9	3.2	0.1	3.8	0.5	43.9	0.3	1.1	0.1
+1	0.0	0.0	0.2	0.2	0.6	25.4	26.9	13.7	7.1	4.3	9.6	8.1	3.8
+2	0.0	0.0	0.0	0.0	0.3	2.1	14.7	21.3	10.9	0.8	23.8	5.6	20.5
+3	0.0	0.0	0.0	0.0	0.9	10.3	5.1	9.7	0.2	0.2	15.3	33.7	24.6
+4	0.0	0.0	0.1	0.1	24.8	10.5	3.2	3.1	31.6	22.6	1.1	2.1	1.0
+5	0.0	0.0	49.7	49.7	0.0	0.1	0.1	0.2	0.0	0.1	0.0	0.1	0.0
+6	50.0	50.0	0.0	0.0	0.0	0.0	0.0	0.0	0.0	0.0	0.0	0.0	0.0

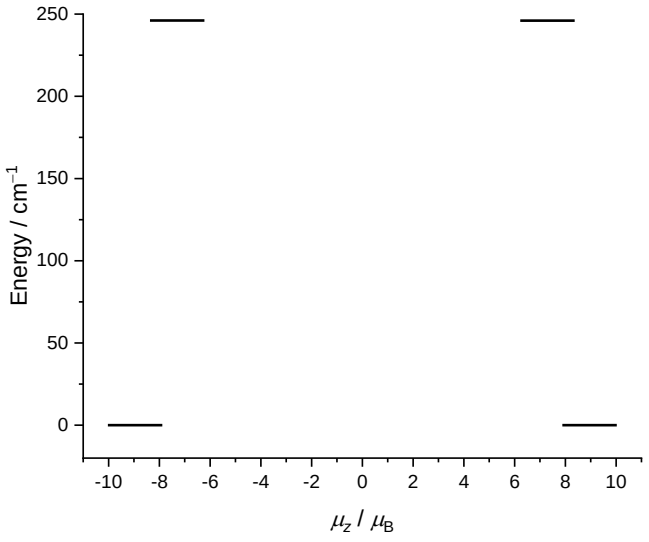

Figure S6. Energy diagram of the lowest and first excited quasi-doublet of **1**.

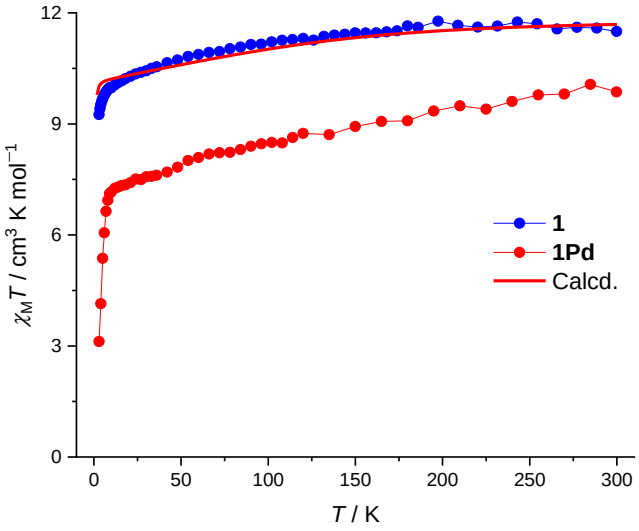

Figure S7. $\chi_M T$ vs. T plots for **1** and **1Pd** under dc magnetic field of 1000 Oe. Theoretical curve derived from ab initio calculation of **1** is shown for comparison. $\chi_M T$ values for **1Pd** were calculated based on the composition of $[C_{72}H_{40}N_{16}TbPd][PdCl_4]$. Small $\chi_M T$ values of **1Pd** compared with the expected value for Tb^{3+} (11.8 cm^3 K mol^{-1}) implies diamagnetic impurity in the powder sample of **1Pd**. Sudden decrease of $\chi_M T$ value of **1Pd** at low T-region indicates the antiferromagnetic interactions and magnetization blocking.

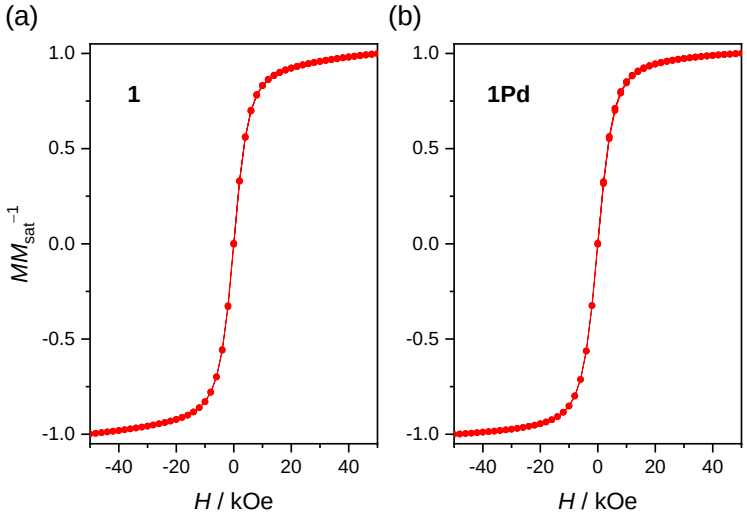

Figure S8. Normalized magnetization curves for (a) **1** and (b) **1Pd** at 2 K. No hysteresis behaviour was observed in both samples.

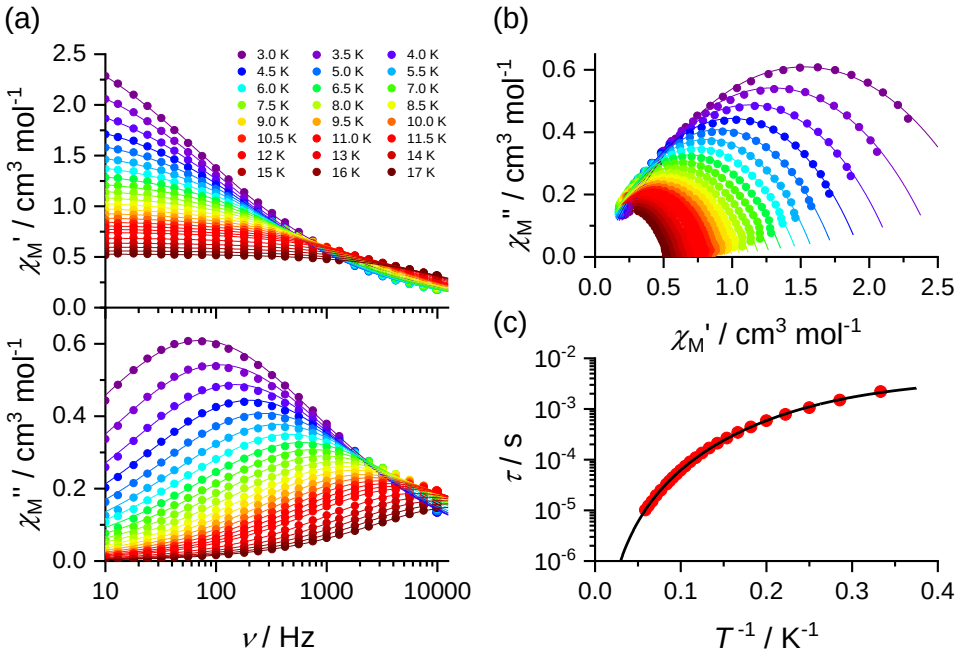

Figure S9. (a) AC magnetic susceptibility and (b) Argand plots for **1** in a zero dc magnetic field. Solid curves represent a fit using generalized Debye model. (c) *T*-dependence of the τ in a zero dc magnetic field. Solid curve represents a fit using the model shown in the text.

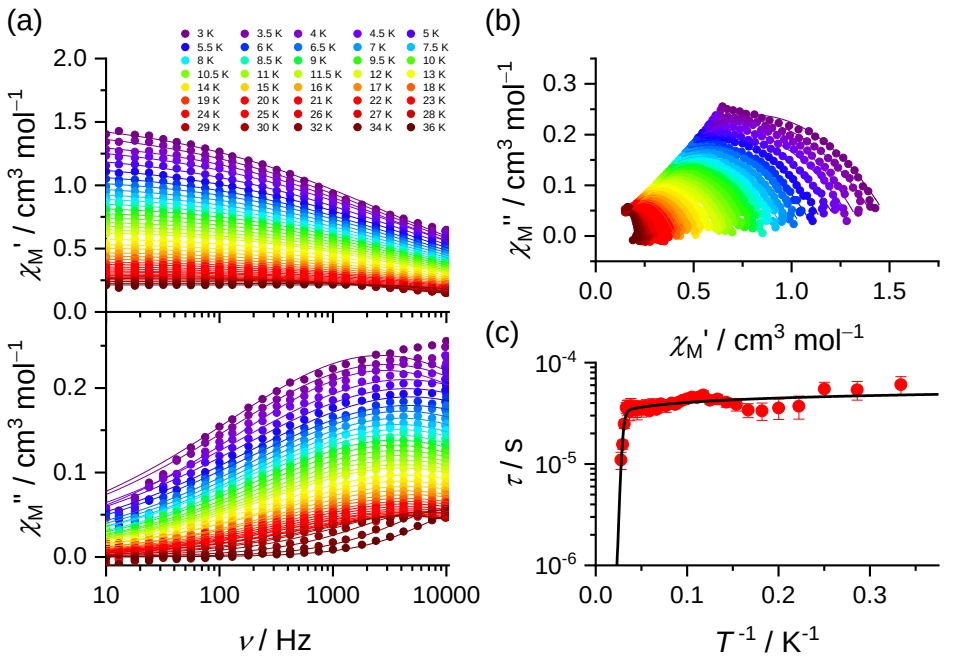

Figure S10. (a) AC magnetic susceptibility and (b) Argand plots for **1Pd** in a zero dc magnetic field. Solid curves represent a fit using generalized Debye model. (c) *T*-dependence of the τ in a zero dc magnetic field. Solid curve represents a fit using the model shown in the text.

Table S1. Parameters obtained by fitting the χ_M' and χ_M'' vs. ν plots of 1 at zero dc field using generalized Debye model.

T / K	τ / μs	χ_S / cm^3 mol^{-1}	χ_T / cm^3 mol^{-1}	α
3	2.2(3) × 10^3	9.3(4) × 10^{-2}	2.95(1)	0.487(2)
3.5	1.49(2) × 10^3	7.9(4) × 10^{-2}	2.51(1)	0.466(3)
4	1.06(1) × 10^3	6.4(4) × 10^{-2}	2.187(8)	0.452(3)
4.5	7.81(9) × 10^2	5.0(4) × 10^{-2}	1.947(7)	0.442(3)
5	5.85(6) × 10^2	3.7(4) × 10^{-2}	1.758(6)	0.437(3)
5.5	4.43(5) × 10^2	2.5(5) × 10^{-2}	1.604(5)	0.433(4)
6	3.43(4) × 10^2	0	1.484(4)	0.436(4)
6.5	2.66(4) × 10^2	0	1.377(5)	0.435(5)
7	2.11(4) × 10^2	0	1.282(5)	0.431(5)
7.5	1.69(3) × 10^2	0	1.200(4)	0.427(5)
8	1.35(3) × 10^2	0	1.129(4)	0.425(6)
8.5	1.09(3) × 10^2	0	1.061(4)	0.418(7)
9	90(2)	0	1.002(3)	0.410(6)
9.5	74(2)	0	0.951(3)	0.408(6)
10	62(2)	0	0.902(3)	0.399(7)
10.5	52(1)	0	0.858(2)	0.393(6)
11	44(1)	0	0.818(2)	0.385(7)
11.5	38(1)	0	0.782(2)	0.380(6)
12	32.7(8)	0	0.750(1)	0.375(5)
13	25(7)	0	0.691(1)	0.363(5)
14	19.5(7)	0	0.641(1)	0.354(6)
15	15.1(6)	0	0.600(1)	0.354(7)
16	12.3(5)	0	0.562(1)	0.348(6)
17	10.2(6)	0	0.529(1)	0.346(8)

Fitting with generalized Debye model was performed with the constraint in that fitting parameters are greater than or equal to zero. Zero values on the table represent that fitting parameters adopt zero under this constraint.

Table S2. Parameters obtained by fitting the χ_M' and χ_M '' vs. ν plots of 1Pd at zero dc field using generalized Debye model.

T / K	τ / μs	χ_S / cm^3 mol^{-1}	χ_T / cm^3 mol^{-1}	α
3	6(1) × 10	8(7) × 10^{-2}	1.54(2)	0.60(2)
3.5	5(1) × 10	6(7) × 10^{-2}	1.48(2)	0.60(2)
4	55(9)	0.11(6)	1.38(1)	0.57(2)
4.5	4(1) × 10	0	1.35(2)	0.62(2)
5	36(8)	0	1.28(2)	0.62(2)
5.5	33(7)	0	1.20(1)	0.61(2)
6	34(5)	2(4) × 10^{-2}	1.14(1)	0.61(1)
6.5	39(5)	7(4) × 10^{-2}	1.073(9)	0.58(2)
7	41(4)	9(3) × 10^{-2}	1.020(6)	0.57(1)
7.5	44(5)	0.11(2)	0.972(6)	0.56(1)
8	42(3)	9(2) × 10^{-2}	0.936(5)	0.56(1)
8.5	48(5)	0.13(2)	0.889(6)	0.54(1)
9	45(4)	0.12(2)	0.851(4)	0.54(1)
9.5	46(4)	0.12(2)	0.807(4)	0.53(1)
10	44(4)	0.12(2)	0.772(4)	0.53(1)
10.5	43(4)	0.11(2)	0.735(4)	0.53(1)
11	41(3)	0.11(1)	0.704(3)	0.53(1)
11.5	39(4)	0.10(2)	0.675(4)	0.54(1)
12	40(3)	0.10(1)	0.648(3)	0.53(1)
13	37(5)	0.10(2)	0.595(4)	0.53(2)
14	39(4)	0.11(1)	0.547(3)	0.50(1)
15	35(3)	8(1) × 10^{-2}	0.522(2)	0.54(1)
16	38(6)	0.10(2)	0.480(4)	0.50(2)
17	33(3)	8.5(8) × 10^{-2}	0.455(2)	0.52(1)
18	37(6)	0.10(2)	0.426(3)	0.49(2)
19	35(4)	9(1) × 10^{-2}	0.402(2)	0.49(2)
20	35(6)	0.10(2)	0.382(3)	0.48(3)
21	36(6)	0.10(1)	0.362(3)	0.46(3)
22	34(7)	9(2) × 10^{-2}	0.345(3)	0.46(3)
23	34(5)	9(1) × 10^{-2}	0.329(2)	0.45(2)
24	36(5)	9(1) × 10^{-2}	0.321(2)	0.46(2)
25	36(6)	9(1) × 10^{-2}	0.304(3)	0.43(3)
26	36(8)	9(2) × 10^{-2}	0.293(3)	0.42(4)
27	33(6)	8(1) × 10^{-2}	0.288(3)	0.45(3)
28	37(6)	9(1) × 10^{-2}	0.273(2)	0.37(4)
29	36(6)	9(1) × 10^{-2}	0.266(2)	0.34(4)
30	36(4)	0.102(9)	0.254(2)	0.26(4)
32	25(2)	9.7(8) × 10^{-2}	0.240(1)	0.19(3)
34	16(2)	9.6(9) × 10^{-2}	0.2258(9)	9(3) × 10^{-2}
36	11(2)	0.11(2)	0.213(1)	0
38	6(3)	9(4) × 10^{-2}	0.2029(7)	0

Fitting with generalized Debye model was performed with the constraint in that fitting parameters are

greater than or equal to zero. Zero values on the table represent that fitting parameters adopt zero under this constraint.

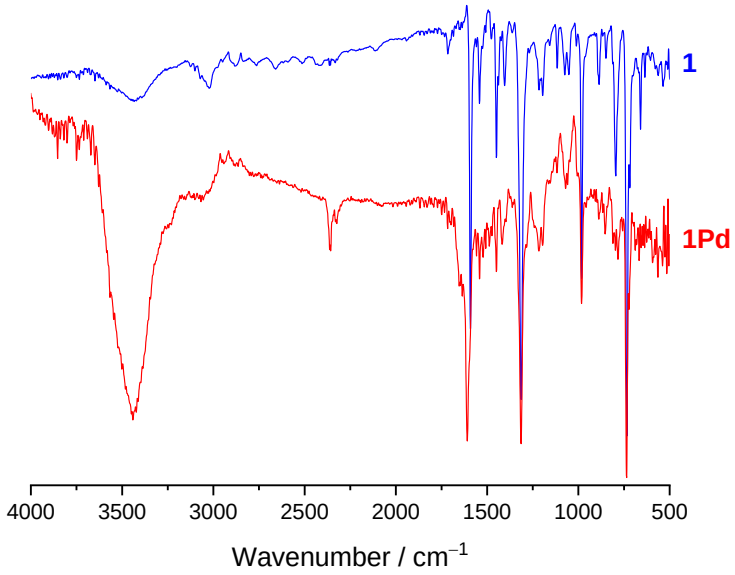

Figure S11. Transmittance FT/IR spectra of **1** and **1Pd** acquired using KBr pellet method.

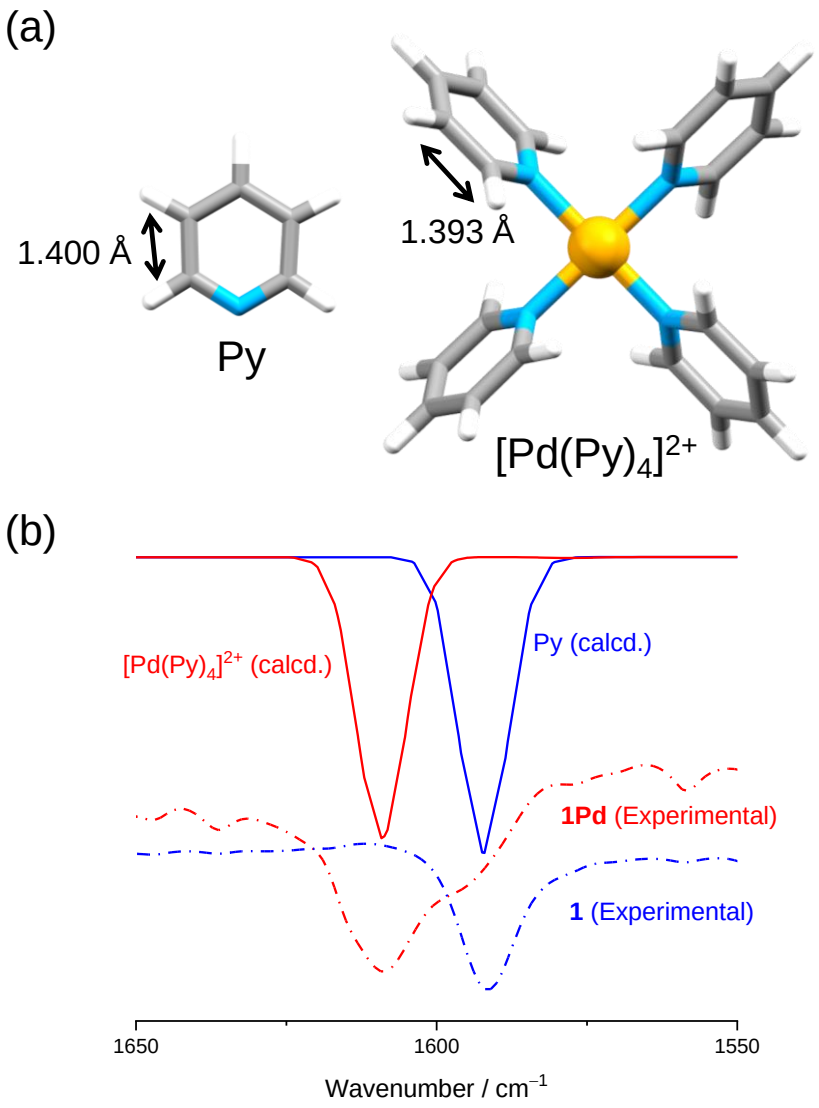

Figure S12. (a) Geometry optimized structure of Py and $[Pd(Py)_4]^{2+}$ and their C=C bond length at B3LPY/Def2-SVP level. (b) Calculated IR transmittance spectra of Py and $[Pd(Py)_4]^{2+}$ in the region of the C=C vibrational mode. The frequency is multiplied by 0.972. Experimental IR spectra are shown for comparison.

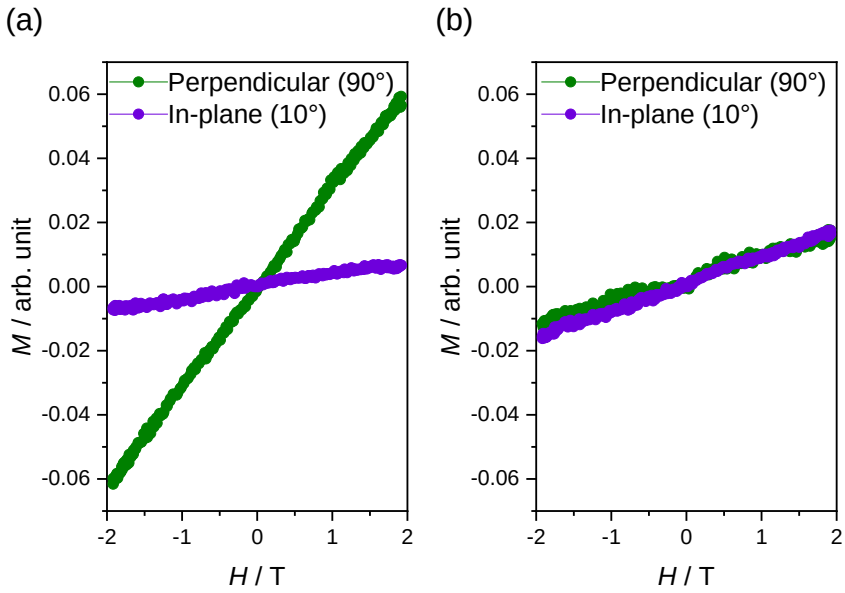

Figure S13. *M* vs. *H* plots of (a) **1Pd** and (b) **1** on the Si wafer derived from normalized XMCD intensity.

References

1. N. Ishikawa, T. Iino and Y. Kaizu, *J. Am. Chem. Soc.*, 2002, **124**, 11440-11447.
2. D. Aravena, F. Neese and D. A. Pantazis, *J. Chem. Theory Comput.*, 2016, **12**, 1148-1156.
3. F. Weigend and R. Ahlrichs, *Phys. Chem. Chem. Phys.*, 2005, **7**, 3297-3305.